# Transition from Internal to External Oxidation in Binary Fe–Cr Alloys Around 900 °C

(article starts on next page)

**RESEARCH**

# Transition from Internal to External Oxidation in Binary Fe–Cr Alloys Around 900 °C

**A. Chyrkin[1] · J. Froitzheim[1] · W. J. Quadakkers[2]**

## Abstract

The transition from external to internal oxidation of a binary Fe-10Cr alloy has been investigated in Fe/FeO Rhines pack (RP) and $H_2/H_2O$ between 850 and 900 °C. Internal oxidation is facilitated by increasing temperature and presence of water vapor. A classical Wagnerian diffusion analysis predicts external oxidation for ferritic (BCC) Fe-10Cr and internal oxidation for austenitic (FCC) Fe-10Cr. The α-to-γ transformation is demonstrated to be the primary factor promoting internal oxidation in Fe–Cr around 900 °C. Water vapor is believed to promote internal oxidation due to a higher reactivity of $H_2O$ compared to $O_2$ and higher preferential adsorption of the $H_2O$ molecule.

## Introduction

High-Cr ferritic steels rely for oxidation protection on the development of chromia scales which form on the alloy surfaces by selective oxidation of Cr during high-temperature exposure. Selective oxidation of Cr to form a continuous $Cr_2O_3$ films is generally found to be retarded in atmospheres containing water vapor [1–3]. This effect often manifests itself in the case of Fe–Cr alloys with intermediate-Cr contents (10–20%) as a phenomenon termed breakaway oxidation. It is frequently observed that alloys which form protective chromia-base scales in air or dry, oxygen-base gases, exhibit breakaway-type oxidation in water–vapor-rich gases due to

✉  A. Chyrkin
   chyrkin@chalmers.se

1   Department of Chemistry and Chemical Engineering, Chalmers University of Technology, Kemivägen 10, 412 58 Gothenburg, Sweden

2   Institute for Energy Materials and Devices (IMD-1), Formerly with Forschungszentrum Jülich GmbH, Leo-Brandt-Straße, 524 25 Jülich, Germany

formation of Fe-rich oxide scales accompanied by internal oxidation. This can result in the oxidation rate in the wet gas being three to five orders of magnitude higher than that in the dry gas [1, 4, 5].

A special type of high-temperature corrosion system in which Fe–Cr alloys are commonly applied is encountered in solid oxide fuel cells (SOFCs) [6] and solid oxide electrolysis cells (SOECs) [7]. The former provides electricity with a high efficiency while the latter allows to produce hydrogen or synthetic fuels required to transform into a low carbon society. In both cases, the essential building block, a stack, consists of many individual cells that are connected in series. Between the cells, metallic interconnects are placed which commonly comprise of ferritic steel [8]. The corrosion environment of these interconnects differs from most other high-temperature applications in that one side of the metal sheet is exposed to air or an oxygen-rich gas while the other side is exposed to a $H_2/H_2O$ environment potentially mixed with CO, $CO_2$ and hydrocarbons [9, 10]. Several authors [11–16] have shown that oxidation under such dual atmosphere conditions differs from oxidation in a single atmosphere, i.e., the same atmosphere on both sides. It is nowadays firmly established that hydrogen from the $H_2/H_2O$ side of the cell diffuses through the metal and results on the air/oxygen side of the cell in an oxidation behavior that is similar to that observed in wet air or wet oxygen. A similar dual atmosphere effect was observed in heat exchanger tubes made of martensitic 9% Cr steel where the air side oxidation at 650 °C was adversely affected by the presence of steam at the tube inside [15, 16].

For explaining the adverse effect of water vapor on the oxidation behavior in $O_2$-rich environments, especially the hampered selective oxidation, of chromium of ferritic steels in air or oxygen a number of mechanisms haven been proposed: (i) reactive Cr(VI)-evaporation [17–19], (ii) modification of transport properties in the $Cr_2O_3$ scale by $H^+$ and/or $OH^-$ [20], (iii) preferential adsorption of $H_2O$ molecules [2], (iv) $H_2O/H_2$ bridges promoting oxygen transport in oxide voids [21], (v) dissolution of hydrogen into the metal increasing oxygen permeability [4, 22, 23].

The latter mechanism was derived from studies in which Fe-10 wt. %Cr showed at 900 °C and above external scale formation in Ar-$O_2$ but solely internal oxidation in an Ar-4%$H_2$ gas containing around 2% $H_2O$ [4]. Similar effects of hydrogen facilitating internal oxidation of Fe–Cr alloys were reported by Ueda et al. [24, 25]. Rhines pack experiments [26] allow to investigate the oxidation behavior in low $pO_2$ atmospheres without the use of reactive gas mixtures such as $H_2/H_2O$ or $CO/CO_2$. This is achieved by placing the samples in an evacuated quartz ampulla with a metal/metal oxide buffer. Once equilibrium is achieved the $pO_2$ in the ampulla corresponds to the dissociation pressure of the chosen metal/metal oxide buffer. Based on experiments comparing the behavior in $H_2/H_2O$ mixtures and Rhines pack, several authors recently questioned the effect of water vapor and hydrogen on the oxygen permeability based on internal oxidation experiments with Fe–Ni–Cr [27–30], Pd–Cr [31] and Fe–2.25Cr [32]. Some of the latter studies were carried out at temperatures that substantially exceed the application range of SOFC/SOEC's, 600–800 °C, while the works by Gunduz et al. [14] and Alnegren et al. [11, 12] have shown that the dual atmosphere effect intensifies with decreasing temperature. Also, the dramatic difference in external

and internal scale formation of Fe-10%Cr in Ar-$O_2$ and Ar-$H_2$.$H_2O$ at 900 °C and above substantially differed from that at lower temperatures [33]. Therefore, extrapolating the conclusions obtained from the observations at 900 °C [4, 22, 23] and above to lower temperatures must be done with utmost precaution. This is especially the case because Fe–Cr alloys with less than 12 wt.-% Cr experience a change from a-ferrite to g-austenite upon a temperature increase above 850 °C. As the transport properties of oxygen and chromium in the α-phase substantially differ from those in the γ-phase, the conditions for protective chromia scale formation may, upon temperature change, be significantly affected by this phase transformation instead of a mere temperature effect on the mentioned diffusivities/permeabilities.

This article opens a series of publications on the role of test environment and the α-to-γ phase transformation on the transition from external scaling to internal oxidation in Fe–Cr alloys during exposure in dry and $H_2$/$H_2O$-based gas mixtures. In the present paper, the isothermal oxidation behavior of Fe-10Cr and Fe-18Cr in Ar-$H_2$-$H_2O$ is compared with that in a Fe/FeO Rhines pack (RP) at temperatures between 850 and 900 °C. Additionally, a dual atmosphere exposure with Fe-10Cr was carried out at 900 °C whereby on one side the oxygen was supplied by RP and on the other side by a Ar-$H_2$-$H_2O$ mixture with the same equilibrium oxygen partial pressure. The obtained oxidation products were characterized using scanning electron microscopy. The results are discussed on the basis of Wagner's analysis for the transition of internal to external chromia scale formation for ferrite and austenite.

## Experimental Procedures

### Materials

The binary model alloys Fe-10Cr and Fe-18Cr (wt. %) were supplied by Sandvik Materials Technology AB (today Alleima AB). The chemical compositions of the alloys are listed in Table 1, the detailed chemical analysis of these alloys can be found elsewhere [3]. The average grain size of the alloys is approximately 50 µm. For the single-atmosphere exposures, test coupons measuring $20 \times 10 \times 2$ mm$^3$ were machined from the ingots. For the dual atmosphere experiments circular specimens were cut from the Fe-10Cr bar. The 0.5 mm thick disks 21.0 mm in diameter were ground with SiC paper to 0.2 mm. All specimen surfaces were polished

**Table 1** Chemical composition of the binary Fe–Cr alloy in wt. % measured by ICP-OES and IR

| Fe | Cr | Al | Ti | Mn | Mo | Ni | Co | Si | C | S |
|----|-----|------|------|------|------|------|------|------|-------|-------|
| Bal | 10.43 | 0.02 | 0.02 | 0.03 | 0.01 | 0.01 | 0.01 | 0.02 | 0.006 | 0.005 |
| Bal | 18.08 | 0.02 | 0.02 | 0.03 | 0.01 | 0.01 | 0.01 | 0.03 | 0.006 | 0.005 |

with diamond paste to 0.25 μm surface finish. The specimens were degreased with acetone and ethanol in an ultrasonic bath and dried with pressurized air prior to exposure.

### Rhines Pack Exposures

The Fe/FeO Rhines pack (hereafter RP) [26] mixture was prepared from an iron powder supplied by BDH Chemicals Ltd (England) adopting a modified procedure described by Prillieux et al. [29]. The iron powder was oxidized in Ar-5H$_2$%-3%H$_2$O at 800 °C for 24 h and dried in flowing argon at 200 °C for 5 h. The alloy coupons were put together with the Fe/FeO mixture in a 16 mm OD quartz tube and sealed under vacuum ($10^{-5}$ mbar). The sealed quartz capsules were exposed in a horizontal tube furnace with a 4 cm wide stable hot zone at the envisaged temperature. The capsules were placed into a cold furnace and heated in stagnant air to the target temperature at 10 K per minute. The capsules were rapidly removed from the hot zone after exposure and cooled in air. The specimens were exposed at 850, 875, 900 °C for 72 h. Selected specimens were additionally exposed for 8, 24 and 168 h.

### H$_2$/H$_2$O Exposures

The H$_2$/H$_2$O exposures were performed in an alumina tube put inside a sealed quartz tube in a horizontal furnace. The Ar-5%H$_2$ gas mixture supplied by Linde Gas was bubbled through a humidifier kept at the envisaged temperature to obtain the gas humidity level, p(H$_2$O) in atm, corresponding to the Fe/FeO equilibrium (see gas compositions in Table 2). The alloy specimens were introduced into the cold furnace, flushed with the dry Ar-5%H$_2$ gas for 1 h and heated at 10 K min$^{-1}$ per minute to reach exposure temperature. The humidification was turned on once the furnace reached the target temperature. The cooling rate was 10 K min$^{-1}$ as well. The gas flow rate was set at 200 ml min$^{-1}$. The exposure temperatures and durations were the same as for the RP exposures.

**Table 2** Partial pressures of oxygen, hydrogen and water vapor prevailing in exposures at the Fe/FeO decomposition level at 850–900 °C

| Exposure temperature / °C | pO$_2$ /bar Fe/FeO | pH$_2$ /mbar | pH$_2$O /mbar | pO$_2$ /bar H$_2$/H$_2$O | Dew point/ °C |
|---|---|---|---|---|---|
| 850 | $1.6 \times 10^{-18}$ | 49 | 24 | $1.5 \times 10^{-18}$ | 20.5 |
| 875 | $5.3 \times 10^{-18}$ | 49 | 25 | $5.2 \times 10^{-18}$ | 21.1 |
| 900 | $1.7 \times 10^{-17}$ | 49 | 26 | $1.7 \times 10^{-17}$ | 21.7 |

Calculated using standard enthalpies and entropies from [66]

## Dual Atmosphere Exposures

In order to differentiate the potential effects of $H_2O$ as an oxidant and hydrogen dissolved in the alloy matrix, dual atmosphere experiments were carried out. A special specimen holder was designed that allows for the simultaneous exposure of the sample with $H_2/H_2O$ on one side and Fe/FeO RP on the other. More details can be found in [32]. A semi-hollow cylindric reactor head, 40 mm OD, with an inner chamber, 16 mm ID, was produced from 253 MA steel and welded to a 6 mm diameter 316 L steel tubes. The inner chamber was stuffed with quartz wool and filled with 2 g of Fe/FeO powder. The circular alloy specimen was clamped with a 253 MA clamping ring. Gold gaskets were used to seal the specimen tightly to the sample holder. Once the specimen was mounted, the inner chamber was purged with Ar at the rate of 50 ml min$^{-1}$ for 1 h. After the purge, the gas inlet was closed while the gas level in the wash-bottle at the outlet was controlled to be stable proving thus the gas tightness of the system. The closed sample holder was placed in a 42 mm ID quartz tube in a horizontal furnace. The quartz tube was tightly closed on one side with a steel flange welded to the connecting tubes and supplied with an O-ring and then flushed with Ar-5%$H_2$ for 1 h at room temperature. While heated to the exposure temperature, the specimen holder released the expanding Ar from the RP chamber into the wash-bottle. Hence, at the test temperature, the inner pressure was maintained at 1 bar. The heating and cooling rate was 10 K min$^{-1}$. The humidification was switched on once the exposure temperature was reached filling thus the quartz tube with the Ar-$H_2$-$H_2O$ mixture (Table 2). The flow rate of Ar-$H_2$-$H_2O$ in the quartz tube was 100 ml min$^{-1}$. The dual atmosphere experiment was carried out at 900 °C for 72 h.

## Microstructural Analyses

The exposed specimens were sectioned, hot-mounted in a conductive Polyfast mounting resin supplied by Struers (Copenhagen, Denmark), subsequently ground with SiC paper to 4000 grit and finally polished to 0.25 mm surface finish. The final ion etching step was performed using the Gatan PECS II System. Alternatively, cross-sections were prepared using the broad-ion beam (BIB) technique using a Leica EM TIC 3X. FEI Quanta 200 ESEM and JEOL JSM-7800F Prime electron microscopes equipped with an energy dispersive X-ray spectrometer (EDS) were used for post-exposure analyses.

## Results

### RP vs $H_2/H_2O$

Figure 1 demonstrates oxygen uptake by Fe-10Cr and Fe-18Cr exposed to $H_2/H_2O$ and RP for 72 h at 850, 875, and 900 °C. For Fe-18Cr, the weight change increases gradually from 0.13 to 0.33 mg/cm$^2$ in the 850–900 °C temperature interval for
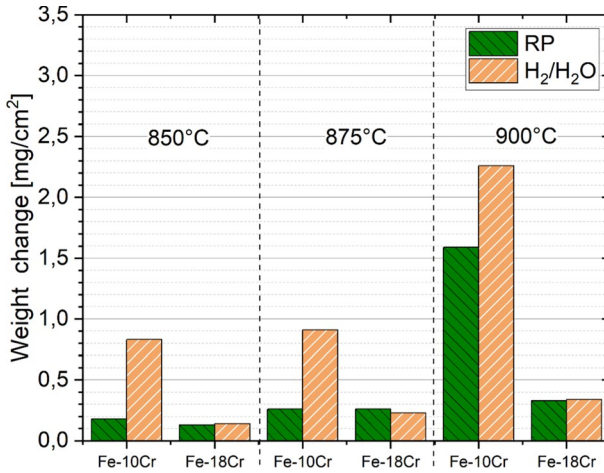
**Fig. 1** Weight change of Fe-10Cr and Fe-18Cr exposed for 72 h to Rhines pack and $H_2/H_2O$, gas compositions in Table 2, at 850, 875 and 900 °C

both RP and $H_2/H_2O$ experiments revealing no difference in oxidation kinetics between the two types of environments. It should be noted that the $pO_2$ changes in this interval by one order of magnitude which is a consequence of the Fe/FeO equilibrium, and the $H_2/H_2O$ ratios were adjusted to match the corresponding $pO_2$ at the respective temperature. The temperature dependence of the parabolic rate constant measured for Fe-18Cr in $H_2/H_2O$ and RP in a broader temperature range, i.e., 800–1000 °C, is presented in Figure A 1 in the Data supplement. In case of Fe-18Cr, no systematic difference between RP and $H_2/H_2O$ has been established.

For Fe-10Cr, two effects can be derived from Fig. 1: (i) oxygen uptakes are systematically higher in $H_2/H_2O$ compared to RP; (ii) weight change dramatically increases between 875 and 900 °C for both environments.

BSE images of cross-sectioned Fe-10Cr after exposures presented in Figs. 2, 3, and 4 illustrate the effect of temperature and the environment on the transition from internal to external oxidation occurring in Fe-10Cr between 850 and 900 °C. At 850 °C (Fig. 2b), the specimen exposed to RP forms a fully external oxide scale while the outer scale grown in $H_2/H_2O$ broke on numerous sites resulting in massive internal oxidation (Fig. 2a). Nonetheless, the outer scale grown in $H_2/H_2O$ still demonstrated a high degree of integrity.

The oxidation products forming in Fe-10Cr during exposure in Ar-$H_2$-$H_2O$ were previously studied in [34]. XRD and Raman spectroscopy identified two phases: $Cr_2O_3$ and $FeCr_2O_4$. Fe-containing spinel is common for outer layers while $Cr_2O_3$ was detected in the innermost parts of the oxidation affected zones. In the present study, a very similar behavior in both RP and $H_2/H_2O$ is observed, i.e., the outer oxide layer has a brighter contrast (spinel) in BSE while the underlying $Cr_2O_3$ has a darker contrast. At 900 °C, the oxide phase in the IOZ is exclusively $FeCr_2O_4$.

Increasing temperature to 875 °C dramatically escalated the unprotective behavior (Fig. 3). The specimen exposed to RP (Fig. 3b) formed a 5.0 μm thick, porous

**Fig. 2** BSE images of cross-sectioned Fe-10Cr alloy specimens exposed for 72 h at 850 °C in **a** $H_2/H_2O$, gas compositions in Table 2, and **b** Fe/FeO RP
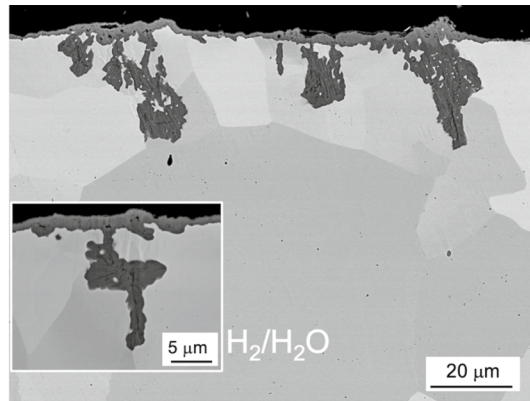


(a)
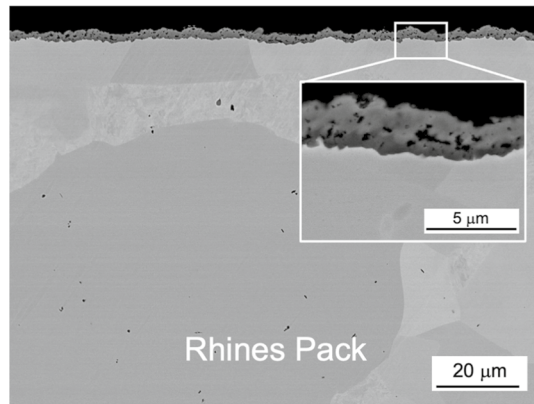


(b)

outer scale. The outer scale shows local breaks (the right-hand side inset in Fig. 3b) marked by an internal oxidation zone (IOZ) healed by a subscale. The $H_2/H_2O$ exposed specimen revealed no external scale at all (Fig. 3a). The internal oxidation morphology had two remarkable features: (i) massive blocks of internal chromia observed in the same environment at 850 °C (Fig. 2a) and (ii) IOZs sealed by a $5 \pm 1$ μm thick subscale.

At 900 °C, Fe-10Cr oxidizes internally in both environments (Fig. 4) in agreement with the previously reported data for $H_2/H_2O$ [22, 23, 34]. Remarkably, the IOZ in the $H_2/H_2O$ is slightly deeper ($33.1 \pm 2.1$ μm after 72 h at 900 °C) than that formed in the RP environment ($29.5 \pm 1$ μm). Although this effect is not strong, it was systematically reproduced in all exposures and previously reported for Fe-5Cr and Fe-10Cr in [24, 25].

To better understand this effect, further exposures of Fe-10Cr at 900 °C for times ranging from 8 to 168 h were undertaken. The temporal evolution of the

**Fig. 3** BSE images of cross-sectioned Fe-10Cr alloy specimens exposed for 72 h at 875 °C in **a** $H_2/H_2O$, gas compositions in Table 2, and **b** Fe/FeO RP. The high magnification insets demonstrate different types of oxide scale morphologies in the same specimen
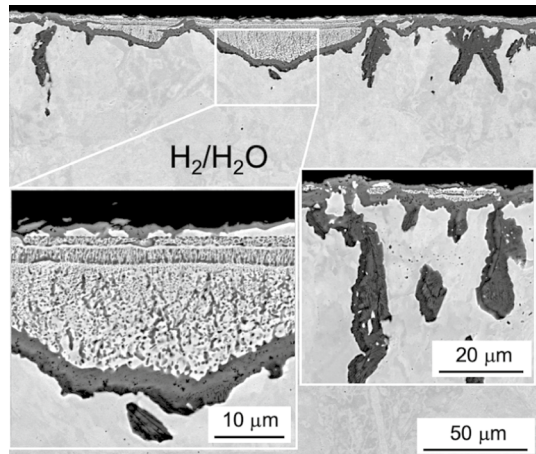


(a)
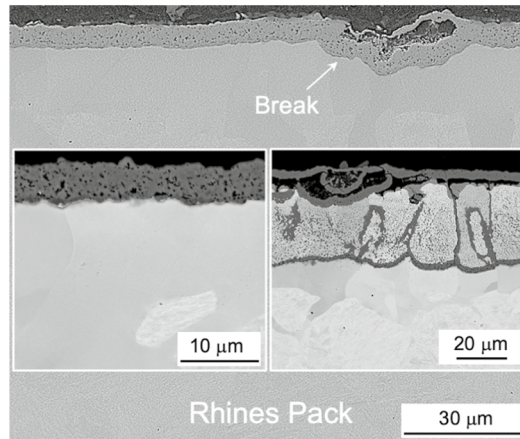


(b)

IOZ in Fe-10Cr in RP and $H_2/H_2O$ growth is displayed in Fig. 5. The internal oxidation kinetics is parabolic being slightly higher for $H_2/H_2O$ compared to RP. The obtained IOZ depth is in good agreement with the data reported in literature [4, 22]. Figure 6 shows oxygen uptake curves for Fe-10Cr at 900 °C exposed to RP and $H_2/H_2O$. In both environments, oxidation kinetics is diffusion controlled and parabolic. The absolute values of oxygen uptake are higher for $H_2/H_2O$ compared to RP.

**Fig. 4** BSE images of cross-sectioned Fe-10Cr specimens exposed for 72 h at 900 °C in **a** $H_2/H_2O$, gas compositions in Table 2, and **b** Fe/FeO RP
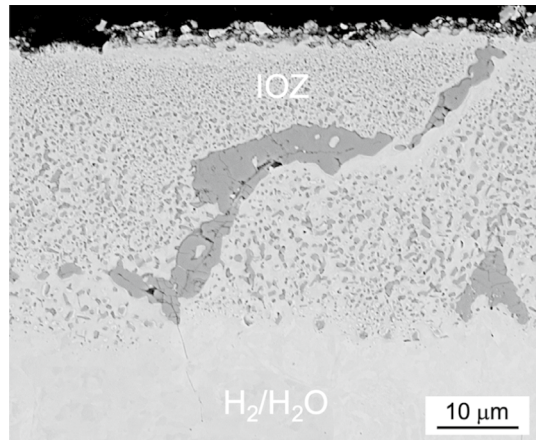


(a)
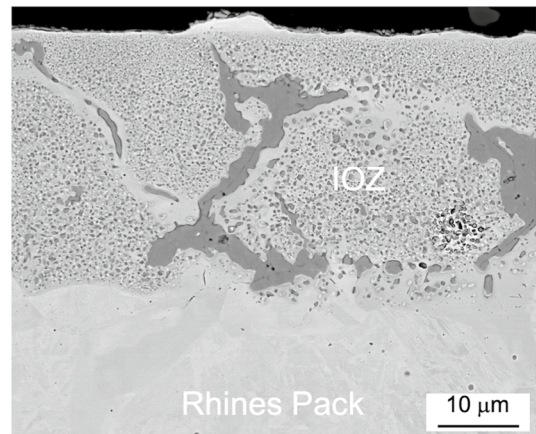


(b)

## Dual Atmosphere

Figure 7a shows an overview BSE image of a 0.2 mm thick Fe-10Cr specimen exposed in dual atmosphere conditions at 900 °C: Fe/FeO RP on one side of the sample and $H_2/H_2O$ on the other. These dual atmosphere experiments were designed in order to differentiate the effect of $H_2O$ from the effect of hydrogen. The latter is expected to rapidly diffuse through the specimen and is hence present also on the RP side [11]. A characteristic internal oxidation morphology was found on both sides, the $H_2/H_2O$-side IOZ being slightly deeper ($29.5 \pm 2$ μm) than the RP-side IOZ ($27.2 \pm 1$ μm). The details of both IOZs are highlighted in high magnification images in Fig. 7b,c. The thicknesses of the IOZs grown in dual atmosphere conditions are in good agreement with those measured in the same conditions in single-atmosphere exposures (compare Fig. 4).
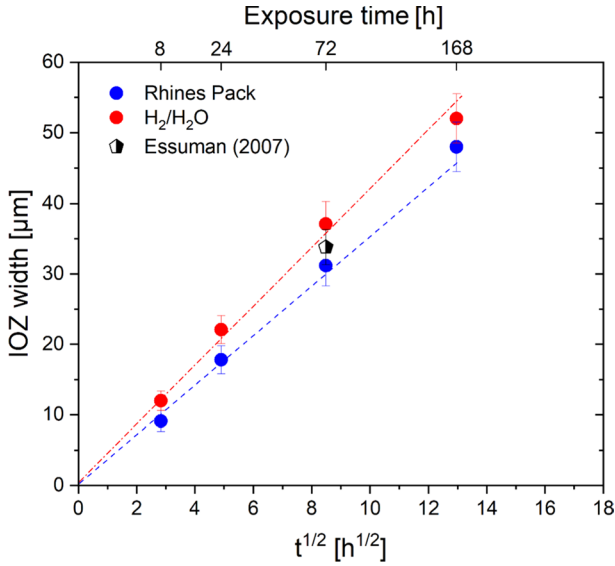
**Fig. 5** Kinetics of internal oxidation in Fe-10Cr exposed in $H_2/H_2O$ (red symbols) and Fe/FeO Rhines pack (blue symbols) at 900 °C
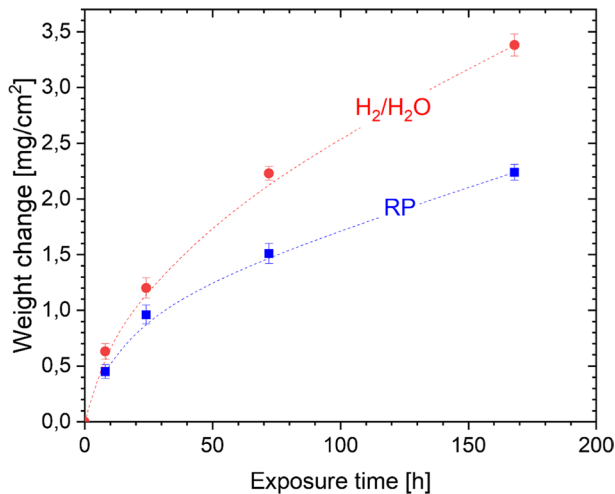


**Fig. 6** Kinetics of oxygen uptake by Fe-10Cr exposed in $H_2/H_2O$ (red symbols) and Fe/FeO RP (blue symbols) at 900 °C

## Effect of $pO_2$

BSE images of cross-sectioned Fe-10Cr specimens after 72-h exposure in Ar-5%-x$H_2O$ are presented in Fig. 8, *x* decreasing from 2.5% in Fig. 8a to 0.01% in Fig. 8d. The exact gas compositions are given in Table 3. Figure 8a reproduces
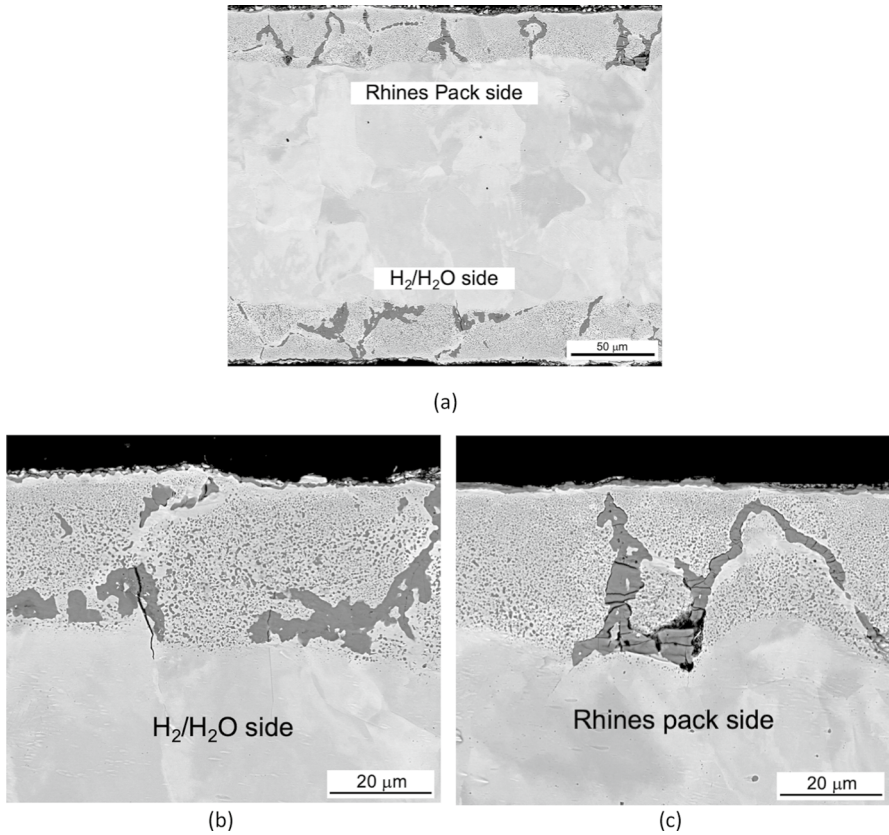
(a)



(b)                                    (c)

Fig. 7 BSE image of cross-sectioned dual atmosphere specimen Fe-10Cr exposed for 72 h at 900 °C: Fe/FeO Rhines pack vs $H_2/H_2O$: **a** overview, **b** $H_2/H_2O$ side, **c** RP side

the microstructure in Fig. 4a, i.e., IOZ with a depth of $33 \pm 1$ μm. Decreasing humidity to 1.5% results in a shallower IOZ ($19 \pm 1$ μm). Below 0.7% $H_2O$, external oxide with a series of internal breaks resembling those in Fig. 2 can be observed.

## Discussion

Two main experimental observations in this study can be summarized as follows:

When Fe-10Cr is oxidized at identical $pO_2$ level in $H_2/H_2O$ and RP at the Fe/FeO equilibrium:

- An abrupt transition from external to internal oxidation occurs close to 900 °C [35].
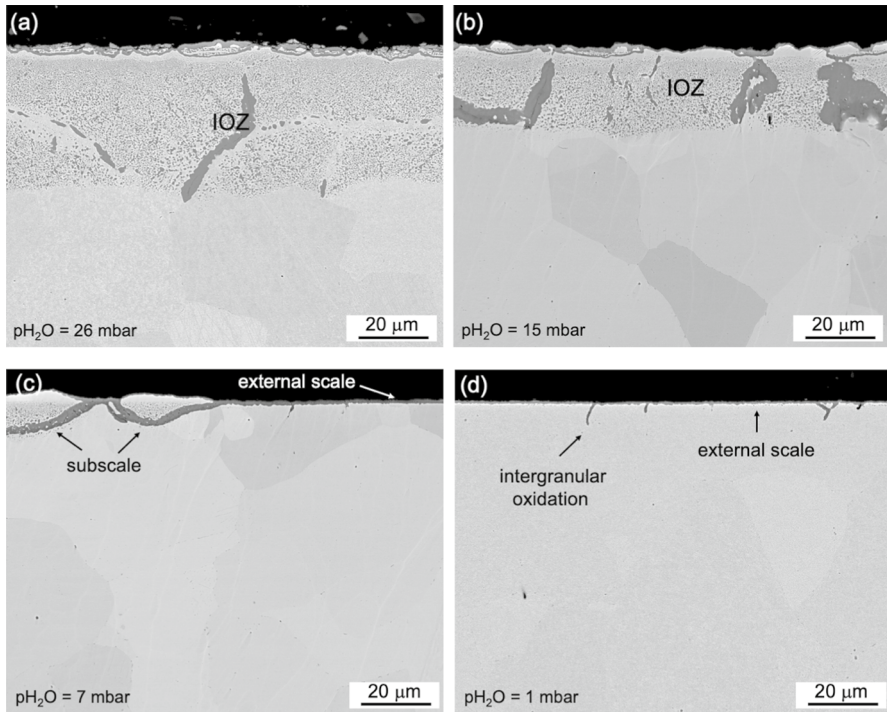
**Fig. 8** Effect of $H_2O/H_2$ ratio (oxygen partial pressure, see also Table 3) on oxidation morphology of Fe-10Cr exposed for 72 h in Ar-$H_2$-$H_2O$ at 900 °C: the $pH_2O/pH_2$ ration is **a** 0.534, **b** 0.305, **c** 0.141, **d** 0.02

- $H_2/H_2O$ facilitates this transition.

The experimental evidence of a detrimental effect of water vapor and hydrogen on protective oxidation of FeCr-base alloys is overwhelming [1, 2, 4, 36–38]. At the same time, Fe-10Cr is expected to be austenitic at 900 °C and above. The austenitic lattice has been previously mentioned as a possible reason for the occurrence of breakaway [39, 40] or internal oxidation [34] in Fe–Cr due to slower Cr diffusion [41, 42] and, hence, a poorer Cr supply to the surface. Therefore, the primary aim of the discussion is to clearly differentiate between

**Table 3** Experimental condition and calculated $N_{Cr}^{crit,1}$ for austenitic Fe–Cr at 900 °C as a function $pH_2O/pH_2$ ratio

| $pH_2O$ / mbar | $pH_2O$ /$pH_2$ | $pO_2$ / bar | $N_O^{(s)}$ | $N_{Cr}^{crit,1}$ | Oxidation morphology |
|---|---|---|---|---|---|
| 26 | 0.534 | $1.7 \times 10^{-17}$ | $6.8 \times 10^{-6}$ | 0.238 | internal |
| 15 | 0.305 | $5.6 \times 10^{-18}$ | $3.5 \times 10^{-6}$ | 0.178 | internal |
| 7 | 0.141 | $1.2 \times 10^{-18}$ | $1.6 \times 10^{-6}$ | 0.121 | borderline |
| 1 | 0.020 | $2.1 \times 10^{-19}$ | $7.1 \times 10^{-7}$ | 0.080 | external |

**Fig. 9** Fragment of binary Fe–Cr phase diagram calculated with Thermo-Calc using the TCFE6 database. Points A, B, C correspond to experiments in Figs. 2–4
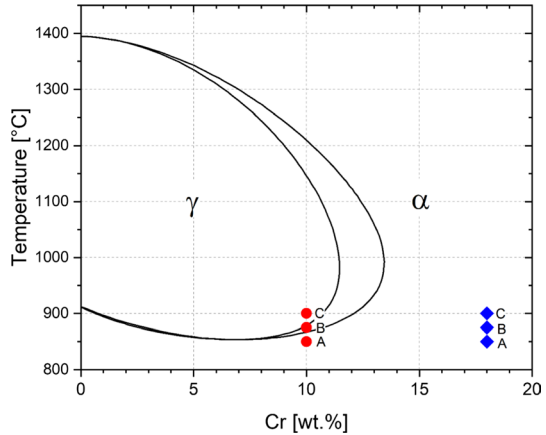
these two effects, i.e., better understand the mechanism behind this temperature dependence and the role of hydrogen and/or water vapor in it.

## Phase Transformation

Figure 9 illustrates a fragment of the Fe–Cr phase diagram calculated in Thermo-Calc using the TCFE6 database [35]. The path A-B-C drawn on the phase diagram indicates a phase composition of the alloy Fe-10Cr at the respective temperature in exposures in Fig. 1. The alloy Fe-10Cr is fully ferritic (BCC) at 850 °C and fully austenitic (FCC) at 900 °C. The calculation predicts the mole-fraction of FCC to be 0.85 in Fe-10Cr at 875 °C. At the same time, Fe-18Cr experiences no phase transformation between 850 and 900 °C and remains fully ferritic.

Considering only the RP exposures first, one can see that the change of the oxidation mode between 850 °C (Fig. 2b – external oxidation) and 900 °C (Fig. 4b) – fully internal oxidation) is dramatic and correlates with the phase transformation in Fe-10Cr between points A and C in Fig. 9. Based on the microscopy results obtained in RP, it seems clear that austenitization of Fe-10Cr is the key factor governing the transition from external to internal oxidation, presumably, further aggravated by the presence of water vapor. In other words, no presence of $H_2/H_2O$ is required to induce internal oxidation of Fe-10Cr at 900 °C. To quantitatively strengthen this statement, a Wagnerian diffusion analysis for both BCC and FCC to compute critical concentrations of Cr required to promote external scaling will be discussed in the next section.

## Wagnerian Criteria

The observations presented in the present study will be discussed in terms of the classical theories of internal [43] and selective external [44, 45] oxidation developed by Carl Wagner. These flux-balance models are extremely popular tools to interpret breakaway

oxidation of FeCr- and NiCr-base alloys in gases containing water vapor [4, 46, 47] compared to dry air and oxygen.

Wagner elaborated two criteria for the formation and maintenance of an external oxide scale on a binary alloy A–B in which $B$ can react with oxygen to form oxide $BO_\mu$ while A remains inert.

The first criterion, given by Eq. (1), predicts the minimum concentration of $B$ in the alloy necessary to overcome the inward ingress of oxygen dissolved in metal by outward Cr diffusion preventing thereby internal oxidation.

$$N_B^{crit,1} > \left[ \frac{\pi g^*}{3} \frac{\overline{V}_m}{\overline{V}ox} \frac{N_O^{(s)} D_O}{\tilde{D}_B} \right]^{\frac{1}{2}} \tag{1}$$

here $N_O^{(s)}$ is the oxygen solubility in the alloy in terms of mole-fraction, $D_O$ is the diffusivity of oxygen in m$^2$ s$^{-1}$, $\tilde{D}_B$ is the interdiffusion coefficient of B in m$^2$ s$^{-1}$, $\overline{V}_m$ and $\overline{V}ox$ are the molar volumes of the alloy and oxide in m$^3$ mol$^{-1}$, respectively. The internal oxide in the Fe–Cr system is chromia, thus, the $\overline{V}_m$ and $\overline{V}ox$ are $7 \times 10^{-6}$ and $15 \times 10^{-6}$ m$^3$ mol$^{-1}$, respectively. The factor $g^*$ is postulated as the minimum volume-fraction of internal oxide to induce the transition from internal oxidation to external scaling and has been approximated by Rapp [48] as 0.3.

The second Wagnerian criterion was derived from a depletion model and predicts the minimum Cr concentration, $N_B^{crit,2}$, in the alloy to sustain the protective $Cr_2O_3$ scale once an external oxide layer has been formed. The second criterion can be expressed as

$$N_B^{crit,2} > \left( \frac{\pi k_c}{2\tilde{D}_B} \right)^{\frac{1}{2}} \tag{2}$$

where $k_c$ is the parabolic rate constant in terms of metal recession in m$^2$ s$^{-1}$.

Both Wagnerian criteria are based on balancing competing fluxes, the latter being expressed via independently measurable transport properties, i.e., oxygen solubility and diffusivity, diffusion coefficient of $B$ and oxidation rate constant. Such a straightforward formulation of the problem offers an easy mechanistic way to analyze the factors governing the transition of protective to no-protective oxide and hence allow to interpret the role of water vapor in breakaway oxidation as the effect of $H_2O$ molecules and/or dissolved H on the above-mentioned transport phenomena resulting in increased $N_B^{crit,1}$ or $N_B^{crit,2}$.

A practical application of Eqs. (1) and (2) to FeCr-base alloys encounters, however, the following challenges: i) oxidation of Fe in high-pO$_2$ gases (i.e., both alloying elements oxidize) which can be circumvented by exposures in low-pO$_2$ atmospheres such as $H_2$/$H_2O$ or RP or taken into account using the approach by Gesmundo and Viani [49], (ii) accuracy of input data, (iii) enhanced diffusion along precipitate surfaces such as in Ni–Al alloys [50]

## Critical Review of Input Data

Being formulated as a square root of $N_O^{(s)}D_O/\widetilde{D}_{Cr}$ or $k_c/\widetilde{D}_{Cr}$, Wagnerian criteria should not be too sensitive to a reasonable variation of these parameters within the measurement error as provided by experiment. However, discrepancies in the available experimental data may often exceed an order of magnitude and thus deserve a separate discussion.

In the present study, the $k_c$ values are directly measured in our own experiments (Figure A 1 in Data supplement). The $\widetilde{D}_{Cr}$ values for BCC were taken from [40] which were in very good agreement with later interdiffusion measurements in [41] and [42]. The accuracy of the selected $\widetilde{D}_{Cr}$ values as well as the $k_c/\widetilde{D}_{Cr}$ ratios were experimentally validated via Cr depletion measurements from experimental Cr concentration profiles in ferric Fe–Cr alloys and a DICTRA simulation using TCFE6 [35] and MOB2 databases [51] (Figure A 2 in Data supplement and Table 4). The oxygen permeability, $N_O^{(s)}D_O$, data for ferritic iron can be taken from several sources [25, 52–54]. For all these studies discrepancies do not exceed a factor of two. The classical dataset by Swisher and Turkdogan [52] with the highest $N_O^{(s)}D_O$ values is preferred as the worst-case scenario for suppression of protective external scale formation.

The choice of data for austenitic iron is more difficult. The $\widetilde{D}_{Cr}$ data for FCC in [4] were taken from [40] which were in turn quoted from [55]. These values are much higher than the interdiffusion coefficients reported by Alberry et al. [41] or Williams and Faulkner [42] and predict external scaling for Fe-10Cr at 900 and 1000 °C [4], i.e., both Wagnerian criteria are fulfilled. The interdiffusion data measurements in [42] were often undertaken on Fe–Cr-Ni alloys and/or commercial austenitic steels. The state-of-the-art CALPHAD diffusion dataset for the Fe–Cr-Ni system is based on the assessment of mobilities by Jönsson [56] and agrees well with [42]. To rule out the effect of Ni on the interdiffusion coefficient of Cr, a diffusion couple Fe-10Cr (the model alloy from the present study) vs pure iron was made and exposed for 72 h at 1000 °C (see Figure A 3 and Figure A 4 in Data supplement). An excellent agreement between the measured interdiffusion profile and the calculated one speaks in favor of the most recent measurement by Williams and Faulkner [42], which were used in the present work.

**Table 4** Literature data and calculated $N_{Cr}^{crit,1}$ and $N_{Cr}^{crit,2}$ for ferritic (BCC) binary Fe–Cr alloys at 800–1000 °C

| T (°C) | $N_O^{(s)}D_O$(m²s⁻¹) | $\widetilde{D}_{Cr}$ | $k_c$(m²s⁻¹) | $N_{Cr}^{crit,1}$ | $N_{Cr}^{crit,2}$ | $N_{Cr}^0 - N_{Cr}^{int}$ |
|---|---|---|---|---|---|---|
| 800 | $1.6\times10^{-16}$ | $3.0\times10^{-15}$ | $1.7\times10^{-19}$ | 0.089 | 0.010 | 0.01 |
| 900 | $5.1\times10^{-16}$ | $9.0\times10^{-15}$ | $1.8\times10^{-18}$ | 0.093 | 0.018 | 0.02 |
| 1000 | $2.6\times10^{-15}$ | $1.5\times10^{-14}$ | $1.6\times10^{-17}$ | 0.108 | 0.025 | 0.02 |

Oxygen permeabilities for BCC iron were taken from [52]. Cr interdiffusion coefficients in ferrite were taken from [40]. Parabolic rate constants were calculated based on own measurements. Experimental Cr depletion (last column) was measured with EDS

The classical $N_O^{(s)}D_O$ data by Swisher and Turkdogan [52] were also selected for austenitic iron based on the data comparison of the $N_O^{(s)}D_O$ values obtained in internal oxidation experiments by Swisher and Turkdogan [52], Meijering [57] and Jullian and Prillieux [27, 29, 30] presented in [30]. All three datasets agree well with each other in a broad temperature range from 950 to 1350 °C while the data by Takada et al. [53] seem to be underestimated (by a factor of 4–5). Julian et al. discuss a possible reason for such a discrepancy being an unusual RP technique that involved Fe powder, FeO or $Fe_2O_3$ and $Al_2O_3$. Components of such a pack may react to form $FeAl_2O_4$, which may consume FeO and establish a lower $pO_2$ in the pack resulting in lower $N_O^{(s)}D_O$ values.

Recently, Pillai et al. [59] made an extensive analysis of the above-mentioned data sources while treating $N_O^{(s)}$ and $D_O$ separately and discussing the degree of equilibration in the saturation experiments of Swisher and Turkdogan [52] and the accuracy of the measurement technique in the recent oxygen solubility measurements in Fe–Ni-Cr alloys by Jullian et al. [28]. It is difficult to assess which $N_O^{(s)}$ values are more accurate based only on literature. On the other hand, the internal oxidation experiments available in [30, 52, 57] provide reproducible measurements of the product $N_O^{(s)}D_O$, which is required as input for Eq. 1. In this approach, any of the three afore mentioned $N_O^{(s)}D_O$ datasets for FCC iron can be considered trustworthy.

Direct implementation of $N_O^{(s)}D_O$ allows to skip the debate about the actual values of $N_O^{(s)}$ and $D_O$ and thus avoid "cherry picking" of the $N_O^{(s)}$ and $D_O$ values from different datasets to obtain a $N_{Cr}^{crit,1}$ value matching empirical observations.

It is noteworthy that the input diffusion coefficients for Eqs. (1) and (2) are bulk values, i.e., they were obtained for highly coarsened alloys with grain size in the rage of mms or even single-crystals. Recent studies [58] demonstrate that a grain boundary (GB) contribution can be essential event at 1000 °C. Corrections for $\widetilde{D}_B$ incorporating the GB contribution need to be considered when applying Wagner's model if experimental observation strongly depart from the predictions.

## Ferrite vs Austenite

The calculated $N_{Cr}^{crit,1}$ and $N_{Cr}^{crit,2}$ values for BCC and FCC lattices are summarized along with the input data in Table 4 and Table 5, respectively. The $N_{Cr}^{crit,1}$ values for ferrite are identical with those in [4] and predict external oxidation for Fe-10Cr

**Table 5** Literature data and calculated $N_{Cr}^{crit,1}$ and $N_{Cr}^{crit,2}$ for austenitic (FCC) binary Fe–Cr alloys at 800–1000 °C

| $T$ (°C) | $N_O^{(s)}D_O$(m$^2$s$^{-1}$) | $\widetilde{D}_{Cr}$ | $k_c$(m$^2$s$^{-1}$) | $N_{Cr}^{crit,1}$ | $N_{Cr}^{crit,2}$ |
|---|---|---|---|---|---|
| 800 | $1.9 \times 10^{-17}$ | $2.9 \times 10^{-17}$ | $2.0 \times 10^{-19}$ | 0.230 | 0.096 |
| 900 | $1.2 \times 10^{-16}$ | $3.0 \times 10^{-16}$ | $1.8 \times 10^{-18}$ | 0.241 | 0.097 |
| 1000 | $8.7 \times 10^{-16}$ | $2.2 \times 10^{-15}$ | $1.6 \times 10^{-17}$ | 0.248 | 0.106 |

Oxygen permeabilities for FCC iron were taken from [52]. Cr interdiffusion coefficients in austenite were taken from [42]. Parabolic rate constants were calculated based on own measurements

below 1000 °C. The $N_{Cr}^{crit,2}$ values are predicted to be low (1–2 wt. %), which agrees well with the fact that the measured Cr depletion profiles are quite flat.

(Figure A 2 in Data supplement and Table 4).

For austenite, the situation is dramatically different (Table 5): neither $N_{Cr}^{crit,1}$ is clearly not fulfilled for Fe-10Cr at 800–1000°Cr while the $N_{Cr}^{crit,2}$ values for FCC can be considered borderline as they closely approach 10 wt. %. The $N_{Cr}^{crit,1}$ values demonstrate a weak temperature dependence (activation energies for the for $N_O^{(s)}D_O$ and $\widetilde{D}_{Cr}$ both equal 246 kJ/mol) while $N_{Cr}^{crit,2}$ is predicted to slightly increase for both BCC and FCC with temperature (activation energy for $k_c$ is measured to be 299 kJ/mol).

The predicted $N_{Cr}^{crit,1}$ values deserve a separate discussion. At first glance, $N_{Cr}^{crit,1}$ seems to be overestimated, i.e., an austenitic-chromia forming alloy would not require as much as 25 wt. % Cr to form an external $Cr_2O_3$ scale. An empirical minimum Cr concentration to sustain external $C_2O_3$ scaling on austenitic steels is approximately 18 wt. % while abundant experimental evidence proves their ability to form external chromia at 800–900 °C [60]. Earlier screening studies on Fe–Cr-Ni alloys came up with 18 wt. % Cr as a threshold for protective behavior [61]. At the same time, $N_{Cr}^{crit,2}$ is reasonably predicted to be 10 wt. % which agreed well with commonly reported values of Cr depletion in Fe–Cr-Ni and Ni–Cr alloys at 900–1000 °C being 10–12 wt. % [62]. Using the $N_O^{(s)}D_O$ data by Takada et al. [53] one would arrive at $N_{Cr}^{crit,1}= 0.13$. The temptation is high to opt for this dataset. However, the data by Swisher and Turkdogan [52] appear more consistent and reliable as discussed in the previous section.

There is an alternative way to experimentally validate $N_{Cr}^{crit,1}$ for austenitic Fe-10Cr using these two different $N_O^{(s)}D_O$ datasets. For a given temperature, only one parameter in Eq. (1) can be experimentally tuned in a controlled manner, i.e., $N_O^{(s)}$. Oxygen solubility is governed by $pO_2$ which can be accurately adjusted trough the $pH_2O/pH_2$ ratio. Table 3 summarizes the experimental conditions at lower $pH_2O$ along with the respective $N_O^{(s)}$ and $N_{Cr}^{crit,1}$ values. For the given $pH_2$ of 5% or 50 mbar, the calculation correctly predicts internal oxidation at 15 mbar $H_2O$ ($N_{Cr}^{crit,1} = 0.178$), a transitional borderline state at 7 mbar $H_2O$ ($N_{Cr}^{crit,1} = 0.121$), and a pseudo-external behavior at 1 mbar $H_2O$ ($N_{Cr}^{crit,1} = 0.08$). The latter is termed pseudo-external as the second Wagnerian condition is extremely close to the initial concentration of Cr in the alloy ($N_{Cr}^{crit,1} = 0.10$). Nevertheless, the $pO_2$ variation experiment (Fig. 8) very accurately shows the transition point at 7 mbar $H_2O$ and thus validates the classical data by Swisher and Turkdogan [52]. For instance, the $N_O^{(s)}D_O$ dataset by Takada et al. [53] predicts this transition already at 15 mbar $H_2O$, which contradicts the experiment (Fig. 8).

The only remaining issue to address is the $N_{Cr}^{crit,1}$ value for Fe–Cr austenite that appears overestimated (0.245 or 25 wt.%). According to the Fe–Cr phase diagram in Fig. 9, there is no experimental way to test a binary austenitic Fe–Cr alloy containing 25 wt. % Cr unless an austenite stabilizing element such as Ni is introduced to the alloy. In fact, addition of nickel to the alloy is the key to understanding of

such a high $N_{Cr}^{crit,1}$ value predicted by Eq. (1). Nickel is known lo lower $N_O^{(s)}D_O$ in Fe–Cr-Ni alloys as recently quantitatively demonstrated by Prillieux et al. [29] and Julian et al. [30]. According to [27], $N_O^{(s)}D_O$ is lower by a factor of 3–4 in alloys containing 15–25 wt. % Ni. This correction lowers $N_O^{(s)}D_O$ to the level of Takada et al. [53] and leads to $N_{Cr}^{crit,1}$ values ranging from 0.12 to 0.14, in excellent agreement with the observations for austenitic alloys [61]. Thus, the present diffusion analysis leads to two important conclusions:

- The transition from external to internal oxidation of Fe-10Cr at 900 °C in both investigated atmospheres is driven exclusively by the α-to-γ phase transformation. Ferrite can sustain external chromia scaling up to 1000 °C (both $N_{Cr}^{crit,1}$ and $N_{Cr}^{crit,2}$ are fulfilled) while austenite is prone to internal oxidation ($N_{Cr}^{crit,1}$ strongly exceeds 10 wt.% while $N_{Cr}^{crit,2}$ approaches the value).
- Wagnerian criteria quantitatively predict transition from internal to external oxidation for the Fe–Cr system providing that key prerequisites are fulfilled: (i) alloy is binary (no effects of alloying elements on kinetic parameters); (ii) no external oxidation of Fe (pO$_2$ at Fe/FeO level); (iii) correct and independently validated input data are employed.

## Effect of H$_2$/H$_2$O

The predictive success of Wagnerian analysis in the previous section is inspiring. However, the question of discrepancy between RP and H$_2$/H$_2$O remains open.

Two distinct effects of water vapor/hydrogen have been observed in the present study:

1. Higher oxygen uptake in H$_2$/H$_2$O in the ferritic range compared to RP (Fig. 1) predominantly in form of massive internal precipitation (Fig. 2a).
2. Higher oxygen uptake during internal oxidation of the austenitic alloy at 900 °C (Fig. 6) in H$_2$/H$_2$O with respect to RP.

Before discussing the mechanistic nature of these effects, it is necessary to state that these effects are caused by the H$_2$O molecule rather than the H$_2$ molecule present in the atmosphere to which the specimen is exposed. This can be unequivocally concluded based on the results of the dual atmosphere exposures (Fig. 7). There is an abundance of experimental evidence that hydrogen diffuses through the ferritic steel in such dual atmosphere experiments [9, 11–13, 16]. The oxidation morphologies obtained in the dual atmosphere conditions did not deviate from those obtained in single-atmosphere experiments. In other words, hydrogen dissolved in the alloy had absolutely no effect on the depth and morphology of IOZs (Fig. 7b,c). Therefore, the H$_2$O molecule as a source of oxygen should be seen as a promoter of (i) faster external scaling and (ii) higher oxygen uptake.

A higher oxygen uptake at 900 °C in $H_2/H_2O$ is also reflected in a slightly deeper IOZ grown in $H_2/H_2O$ compared to that grown in the RP exposure (Fig. 4). This effect has been previously reported for Fe-5Cr exposed to "dry" (evacuated RP) and "wet" (RP with a certain pressure of $H_2$) environment at 800 °C [24, 25]. Despite the differences in experiment design in [24] and the present study, the effect of $H_2/H_2O$ on internal oxidation Fe–Cr is remarkably reproducible. This observation has earlier been interpreted as an indication for enhanced oxygen permeability during exposure in $H_2/H_2O$ [4, 22, 23]. Our recent experiments in a diluted Fe-2Cr, i.e., an alloy much more suitable for oxygen permeability measurements, revealed no difference of the IOZ depth between $H_2/H_2O$ and RP [32]. Systematic studies in a broad range of compositions in the Fe–Cr-Ni system [27, 29, 30] quantitatively confirmed the independence of oxygen permeability, $N_O^{(s)} D_O$, from the reaction environment. Hence, another explanation needs to be sought.

A higher aggressivity of $H_2/H_2O$ compared to RP in internal oxidation of Fe–Cr may also be a consequence of preferential adsorption of $H_2O$. This mechanism has been previously employed to explain a detrimental effect of humidity during oxidation of ferritic-martensitic steels at 550–650 °C [2]. As oxygen-bearing species, e.g., $O_2$, $H_2O$, $CO_2$, differ in the energy of chemical bonds in the molecules, they may differ in their reactivity with the metal surface, adsorption rates and thus compete when simultaneously present in a corrosive environment. This mechanism finds an empirical confirmation in poisoning experiments [63, 64] in which minor additions of sulfur-bearing species ($SO_2$ or $H_2S$, depending on $pO_2$) promote external oxidation in humid gases. Sulfur is believed to block available adsorption sites and thus drastically reduces the effective oxygen supply by $H_2O$ molecules. Poisoning was introduced to Wagner's theory as a boundary condition in [65] and was quantitatively demonstrated to lower $N_B^{crit,1}$.

An important reservation must be made when discussing the preferential adsorption mechanism with respect to the presented results, i.e., oxidation of Fe–Cr exposed to $H_2/H_2O$ or RP. What is the actual oxygen carrier in an evacuated quartz capsule containing an alloy specimen together with Fe/FeO RP? The oxygen partial pressure at 900 °C set by the Fe/FeO equilibrium is set by the Fe/FeO equilibrium at $1{,}7 \times 10^{-17}$ bar (Table 2) while the residual gas pressure in an evacuated capsule is $10^{-9}$ bar. Even in best state-of-the-art ultra-high vacuum systems ($10^{-12}$ bar), the residual pressure is orders of magnitude higher than $pO_2$ set by the Fe/FeO equilibrium. Hence, it is extremely unlikely that molecular oxygen is the main oxygen-bearing species. A much more realistic option is $H_2O$ serving as an oxygen shuttle [21] in a gas-transport reaction between FeO in the RP and the alloy specimen. In other words, whenever a "dry" oxidation scenario in RP is compared with a "wet" one (in a flowing gas of $H_2/H_2O$), it is always a comparison between a high $pH_2O$ (tens of mbar) and extremely low pressures of water vapor (presumably some pbar).

## Concluding Remarks

The following conclusions can be drawn from this work:

- The transition from external to internal oxidation in Fe-10Cr that occurs around 900 °C is due to the $\alpha$-to-$\gamma$ phase transformation. Even though water vapor has an effect on the external scaling and kinetics of internal oxidation, the main factor promoting internal oxidation is austenitization.
- Classical Wagnerian diffusion analysis accurately predicts the critical concentrations $N_{Cr}^{crit,1}$ and $N_{Cr}^{crit,2}$ for ferritic and austenitic Fe–Cr and thus quantitatively confirms the previous statement.
- Water vapor results in higher oxygen uptakes compared to RP exposure at identical $pO_2$ both in external (ferrite) and internal (austenite) oxidation modes. In the external scenario, $H_2O$ promotes intergranular attack. At the same time, it neither intensifies surface Cr depletion nor leads to a collapse of the external scale grown on a ferritic grain.
- The difference in oxygen uptakes in the two types of test environments is believed to be related to the fact that the surface reaction of oxygen transfer by water vapor molecules is faster than that by oxygen molecules and a much lower pressure of $H_2O$ in the RP environment in which the $H_2O$ molecule is the dominating oxygen-bearing species.

**Data Availability** Data will be made available on a reasonable request.

## Declarations

**Conflict of interest** The authors declare no competing interests.

# References

1. N. K. Othman, J. Zhang, and D. J. Young, *Oxidation of Metals* **73**, 2010 (337).
2. J. Ehlers, D. J. Young, E. J. Smaardijk, et al., *Corrosion Science* **48**, 2006 (3428).
3. B. Pujilaksono, T. Jonsson, H. Heidari, M. Halvarsson, J.-E. Svensson, and L.-G. Johansson, *Oxidation of Metals* **75**, 2011 (183).
4. E. Essuman, G. H. Meier, J. Zurek, M. Hänsel, and W. J. Quadakkers, *Oxidation of Metals* **69**, 2008 (143).
5. N. Mu, K. Jung, N. M. Yanar, et al., *Oxidation of Metals* **79**, 2013 (461).
6. S. Zarabi Golkhatmi, M. I. Asghar, and P. D. Lund, *Renewable and Sustainable Energy Reviews* **161**, 2022 112339.
7. Y. Xu, S. Cai, B. Chi, and Z. Tu, *International Journal of Hydrogen Energy* **50**, 2024 (548).
8. W. J. Quadakkers, J. Piron-Abellan, V. Shemet, and L. Singheiser, *Materials at High Temperatures.* **20**, 2003 (115).
9. G. R. Holcomb, M. Ziomek-Horoz, S. D. Cramer, B. S. Covino, and S. J. Bullard, *Journal of Materials Engineering and Performance* **15**, 2006 (404).
10. A. W. Bredvei Skilbred and R. Haugsrud, *International Journal of Hydrogen Energy* **37**, 2012 (8095).
11. P. Alnegren, M. Sattari, J. E. Svensson, and J. Froitzheim, *Journal of Power Sources* **301**, 2016 (170).
12. P. Alnegren, M. Sattari, J. E. Svensson, and J. Froitzheim, *Journal of Power Sources* **392**, 2018 (129).
13. C. Goebel, P. Alnegren, R. Faust, J. E. Svensson, and J. Froitzheim, *International Journal of Hydrogen Energy* **43**, 2018 (14665).
14. K. O. Gunduz, A. Chyrkin, C. Goebel, et al., *Corrosion Science* **179**, 2021 109112.
15. K. Nakagawa, Y. Matsunaga, and T. Yanagisawa, *Materials at High Temperatures.* **18**, 2001 (51).
16. K. Chandra and A. Kranzmann, *Corrosion Engineering Science and Technology.* **53**, 2018 (27).
17. H. Asteman, J. E. Svensson, and L. G. Johansson, *Oxidation of Metals.* **57**, 2002 (193).
18. D. J. Young and B. A. Pint, *Oxidation of Metals.* **66**, 2006 (137).
19. G. R. Holcomb, *Oxidation of Metals.* **69**, 2008 (163).
20. Norby T. Le, *Journal de Physique IV.* **03**, 1993 (C999).
21. A. Rahmel and J. Tobolski, *Corrosion Sciience* **5**, 1965 (815).
22. Essuman E, Meier GH, Zurek J, Hänsel M, Singheiser L, Quadakkers WJ. 2008 *High Temperature Corrosion and Protection of Materials 7, Pts 1 and 2.* 595:699
23. E. Essuman, G. H. Meier, J. Zurek, M. Hänsel, L. Singheiser, and W. J. Quadakkers, *Scripta Materialia* **57**, 2007 (845).
24. Ani MH. Bin, T. Kodama, M. Ueda, K. Kawamura, and T. Maruyama, *Materials transactions* **50**, 2009 (2656).
25. A. R. Setiawan, M. Hanafi Bin Ani, M. Ueda, K. Kawamura, and T. Maruyama, *ISIJ International.* **50**, 2010 (259).
26. F. Rhines, W. Johnson, and W. Anderson, *Trans Metallergy Society AIME* **147**, 1942 (205).
27. D. Jullian, A. Prillieux, J. Zhang, and D. J. Young, *Materials and Corrosion.* **68**, 2017 (197).
28. D. Jullian, J. Zhang, D. B. Hibbert, and D. J. Young, *Journal of Alloys Compounds* **732**, 2018 (646).
29. A. Prillieux, D. Jullian, J. Zhang, D. Monceau, and D. J. Young, *Oxidation of Metals.* **87**, 2017 (273).
30. D. Jullian, A. Prillieux, D. B. Hibbert, J. Zhang, and D. J. Young, *Corros Sci.* **224**, 2023 111465.
31. A. Chyrkin, C. Cossu, J.-E. Svensson, and J. Froitzheim, *Oxidation of Metals.* **97**, 2022 (527).
32. A. Chyrkin, C. Cossu, J.-E. Svensson, and J. Froitzheim, *Oxidation of Metals.* **98**, 2022 (273).
33. D. J. Young, J. Zurek, L. Singheiser, and W. J. Quadakkers, *Corrosion Science* **53**, 2011 (2131).
34. J. Zurek, G. H. Meier, E. Wessel, L. Singheiser, and W. J. Quadakkers, *Materials and Corrosion.* **62**, 2011 (504).
35. Thermo-Calc. TCFE6 - TCS Steels/Fe-Alloys Database, Version 6.2. 2013;
36. D. J. Young, *Materials Science Forum* **595–598**, 2008 (1189).
37. A. Galerie, J. P. Petit, Y. Wouters, J. Mougin, A. Srisrual, and P. Y. Hou, *Materials Science Forum.* **696**, 2011 (200).
38. T. D. Nguyen, J. Zhang, and D. J. Young, *Corrosion Science* **236**, 2024 112265.

39. Z. Yang, M. S. Walker, P. Singh, and J. W. Stevenson, *Electrochemical and Solid-State Letters.* **6**, 2003 (B35).
40. D. P. Whittle, G. C. Wood, D. J. Evans, and D. B. Scully, *Acta Metallurgica.* **15**, 1967 (1747).
41. P. J. Alberry and C. W. Haworth, *Metal Science.* **8**, 1974 (407).
42. P. I. Williams and R. G. Faulkner, *Journal of Mater Science* **22**, 1987 (3537).
43. C. Wagner, *Zeitschrift fur Elektrochemie.* **63**, 1959 (772).
44. C. Wagner, *Journal of Electrochemicall Soceity.* **99**, 1952 (369).
45. C. Wagner, *Journal of Electrochemical Soceity* **103**, 1956 (571).
46. E. Essuman, G. H. Meier, J. Zurek, et al., *Corrosion Science* **50**, 2008 (1753).
47. G. H. Meier, K. Jung, N. Mu, et al., *Oxidation of Metals.* **74**, 2010 (319).
48. R. A. Rapp, *Acta Metallurgica.* **9**, 1961 (730).
49. N. Birks, G. H. Meier, and F. S. Pettit, Introduction to the High Temperature Oxidation of Metals. *Cambridge University Press, Cambridge* 2006. https://doi.org/10.1017/CBO9781139163903.
50. H. Hindam and D. P. Whittle, *Journal of Materials Science* **18**, 1983 (1389).
51. Thermo-Calc. MOB2 - TCS Alloys Mobility Database, version 2.7. 2009;
52. J. H. Swisher and E. T. Turkdogan, *Trans Metallergy Society AIME.* **239**, 1967 (426).
53. J. Takada and M. Adachi, *Journal of Materials Science* **21**, 1986 (2133).
54. J. Takada, S. Yamamoto, S. Kikuchi, and M. Adachi, *Oxidation of Metals* **25**, 1986 (93).
55. Borisov VT, Solikov VM, Dulinin GN. *Izv. Akad. Nauk S.S.S.R., Mat. i Gorn. Delo.* 1964;147.
56. B. Jönsson, *International Journal of Materials Research.* **86**, 1995 (686).
57. J. L. Meijering, *Acta Metallurgica.* **3**, 1955 (157).
58. T. Gheno, C. Rio, E. Rimpot, and S. Mercier, *High Temperature Corrosion of Materials* **100**, (2023) 709.
59. R. Pillai, Q. Q. Ren, C. J. Stephens, et al., *Materialia (Oxf).* **28**, 2023 101772.
60. H. Buscail, S. El Messki, F. Riffard, S. Perrier, R. Cueff, and C. Issartel, *Journal of Materials Science* **43**, 2008 (6960).
61. Croll JE, Wallwork GR. *Oxidation of Metals 1969 1:1.* 1969;1:55
62. G. C. Wood, T. Hodgkies, and D. P. Whittle, *Compounds of Corrosion Science* **6**, 1966 (129).
63. A. W. Cramb, W. R. Graham, and G. R. Belton, *Metallurgical Transactions B.* **9**, 1978 (623).
64. H. J. Grabke and E. M. Petersen, *Surface Science* **67**, 1977 (501).
65. G. Luckman and R. S. Polizzotti, *Metallurgical Transactions A.* **16**, 1985 (133).
66. I. Barin, F. Sauert, E. Schultze-Rhonhof, and W. S. Sheng, *Thermochemical Data of Pure Substances, Part 1,* (VCH, Ag-Kr, 1993).